Arabian Journal for Science and Engineering (2023) 48:14105–14118
https://doi.org/10.1007/s13369-023-08090-3

RESEARCH ARTICLE-CIVIL ENGINEERING

# Machine Learning-Based Design Approach for Concrete-Filled Stainless Steel Tubular Columns

Adriano Silva de Carvalho[1] · Alexandre Rossi[2] · Samadhan G. Morkhade[3] · Carlos Humberto Martins[4]

Received: 3 April 2023 / Accepted: 19 June 2023 / Published online: 7 July 2023


## Abstract

Concrete-filled steel tubes have become popular due to their desirable properties, including compressive strength, plasticity, and ease of construction. This study aimed to comprehensively analyze the axial response of short columns made of concrete-filled austenitic stainless steel tubes. The different parameters of these columns were carefully evaluated and compared to principal international design codes. This analysis gained a deeper understanding of the structural behavior of concrete-filled stainless-steel tubes under axial compression. Based on the data obtained from the parametric study, two supervised machine learning models were used to model the compression behavior of these elements, the artificial neural networks model and the random forest model. It was observed that the results obtained through machine learning algorithms provide a significantly more accurate response than the models available in design codes. Additionally, it was observed through the study that the best results were achieved with the artificial neural networks model, with a correlation coefficient of 0.99. The trained machine learning models were implemented into software, allowing the prediction of the behavior of these structures in the range of the data presented in the study.

**Keywords** Artificial neural networks · CFST · Axial compression · Stainless steel · Finite element modelling · Random Forest

## 1 Introduction

Concrete-filled steel tubes are gaining popularity in civil construction due to their versatility in a wide range of applications. These structural elements offer various advantages, including high bearing capacity and deformability, which make them a preferred choice in construction projects [1]. It is noteworthy, for example, that this type of composite section is commonly used in tall buildings [2] and usually has large cross-section dimensions. Concrete-filled composite columns come as an alternative to the use of reinforced concrete or steel columns. This is because the composite section makes use of the best characteristics of each of its constituent materials. When the steel profile is filled with concrete, it becomes less susceptible to local instabilities, and the concrete, confined by the steel profile, gains ductility [3].

In this manner, concrete-filled steel tubes offer a viable solution for efficiently constructing buildings that need to withstand seismic activities. This is because conventional reinforced concrete structures are prone to failure due to shear stress under such actions, and traditional steel structures can suffer early instabilities. In such a scenario, composite elements can overcome these problems and provide a more efficient solution. When used to confine the concrete, steel significantly improves its behavior and resistance, making it an ideal choice for seismic-resistant construction projects [4].

Different section geometries can be found in concrete-filled steel tubes, such as circular [5, 6], rectangular [7, 8], hollow sections [9], X-sections [10, 11], and even oval sections [12]. In addition to the visual differences between these types of concrete-filled steel tube geometries, the section

✉ Carlos Humberto Martins
chmartins@uem.br

1 Department of Civil Engineering, Federal University of São Carlos, São Carlos, Brazil

2 Civil Engineering Faculty, Federal University of Uberlândia, Uberlândia, Brazil

3 Department of Civil Engineering, VPKBIET, Savitribai Phule Pune University, Pune, India

4 Department of Civil Engineering, State University of Maringá, Maringá, Brazil

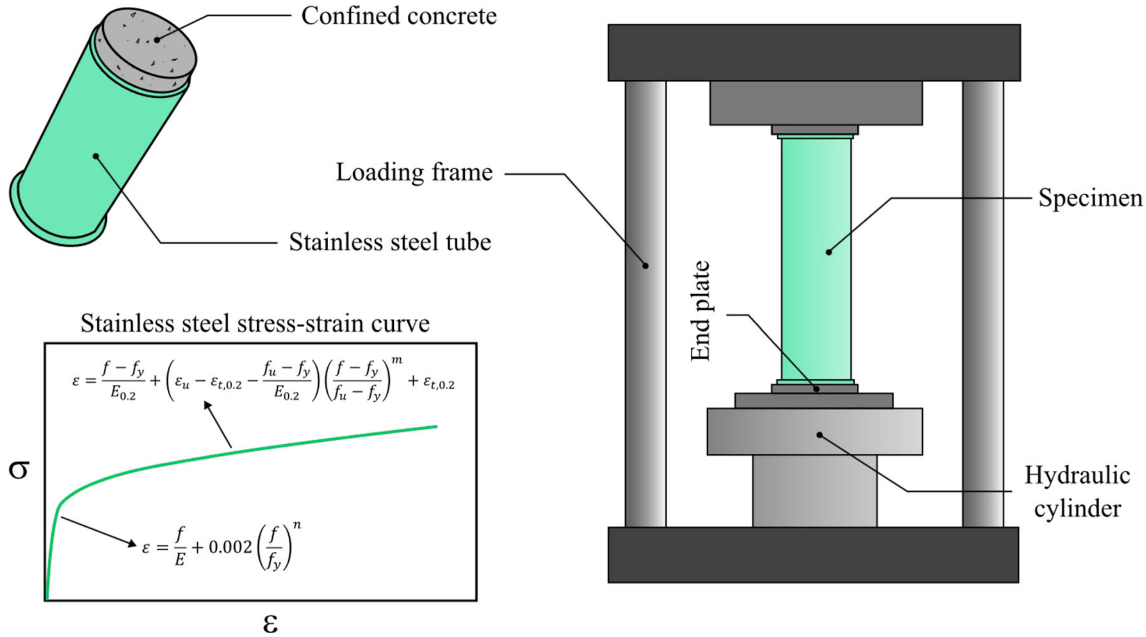


**Fig. 1** Concrete-filled steel tubes with stainless steel outer tubes

**Fig. 2** Finite element mesh

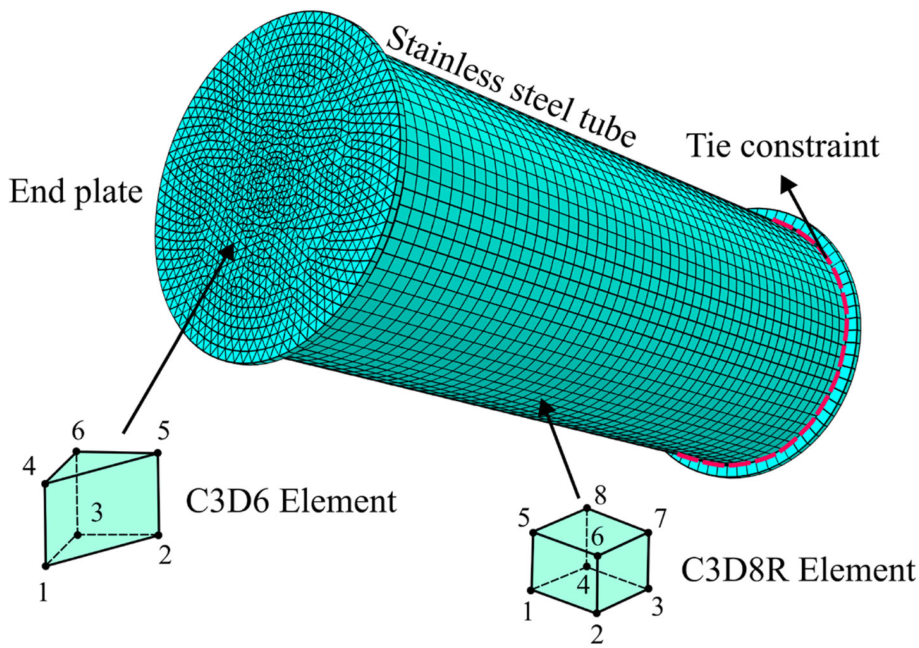


geometry primarily affects the confinement exerted by the steel section in the infill concrete. For example, the confinement effect is significantly greater in circular sections than in rectangular sections because the circular section better distributes the confining pressures. Furthermore, it is known that the confinement effect only manifests once the lateral expansion of the steel equals/exceeds the lateral expansion of the steel tube [13]. This fact can delay the confinement effect, which impairs the action of the steel tube in promoting gains in resistance and ductility to the concrete section present in the filling [13–15]. Due to this, the amount of research on the mechanical behavior of different types of concrete-filled tube geometries has been growing over the last few years, highlighting the execution of experimental tests, computer simulations, and characterization of materials involved in this type of structural member.

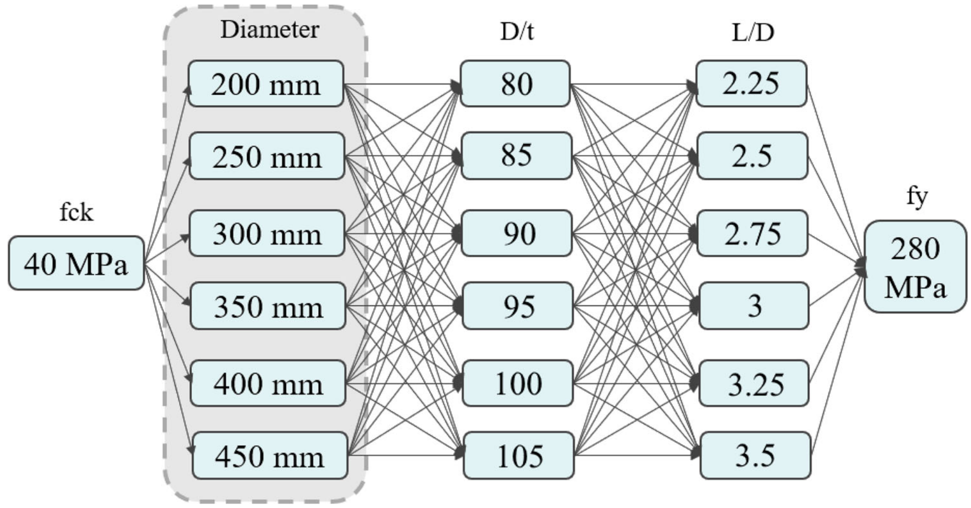


**Fig. 3** Flowchart of the geometric characteristics of the performed analyses

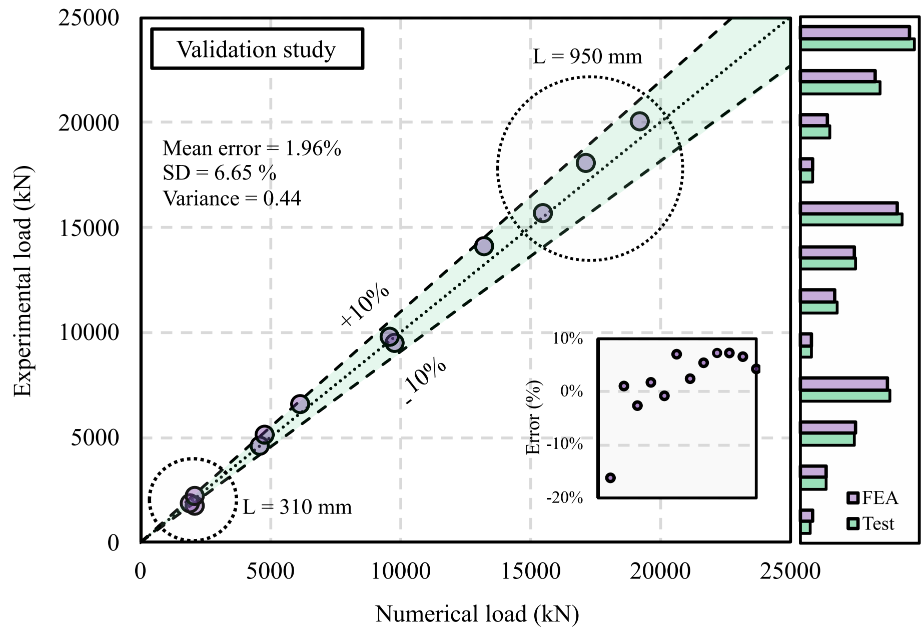


**Fig. 4** Results from the validation study performed

In recent years, stainless steel has emerged as a preferred material for structural applications due to its advantages over carbon steel, including superior corrosion resistance, greater ductility, and enhanced fire resistance. The performance of concrete-filled steel tubes can be improved by incorporating stainless-steel tubes in their construction. Using an external stainless-steel tube in a filled column (as depicted in Fig. 1) can be an effective solution for aggressive environments or situations that may involve fire hazards [16].

A parametric study was conducted using the ABAQUS finite element software package to assess the axial loading response of concrete-filled steel tube (CFST) columns with an austenitic stainless steel outer tube. The behavior of CFST columns was validated using experimental tests conducted by [17] (as shown in Fig. 1), and a total of 216 filled columns with compact sections were analyzed to compose the parametric study. The obtained results were compared against the design codes AISC-360:2016 (United States), EUROCODE 4 (Europe), and AIJ: 2008 (Japan).

Based on the parametric study carried out, it was possible to develop the training of two different machine learning models, the Artificial Neural Network and the Random Forest models. These two machine learning algorithms were widely used in various engineering problems, especially in structural engineering. In this specific case, machine learning models produce a reliable way to estimate several parameters intrinsic to different types of structures, such as their resistant capacity [18, 19], modal parameters [20], displacements [21], and resistance reduction due to high-temperature exposure [22]. Thus, the potential of this type of technique in

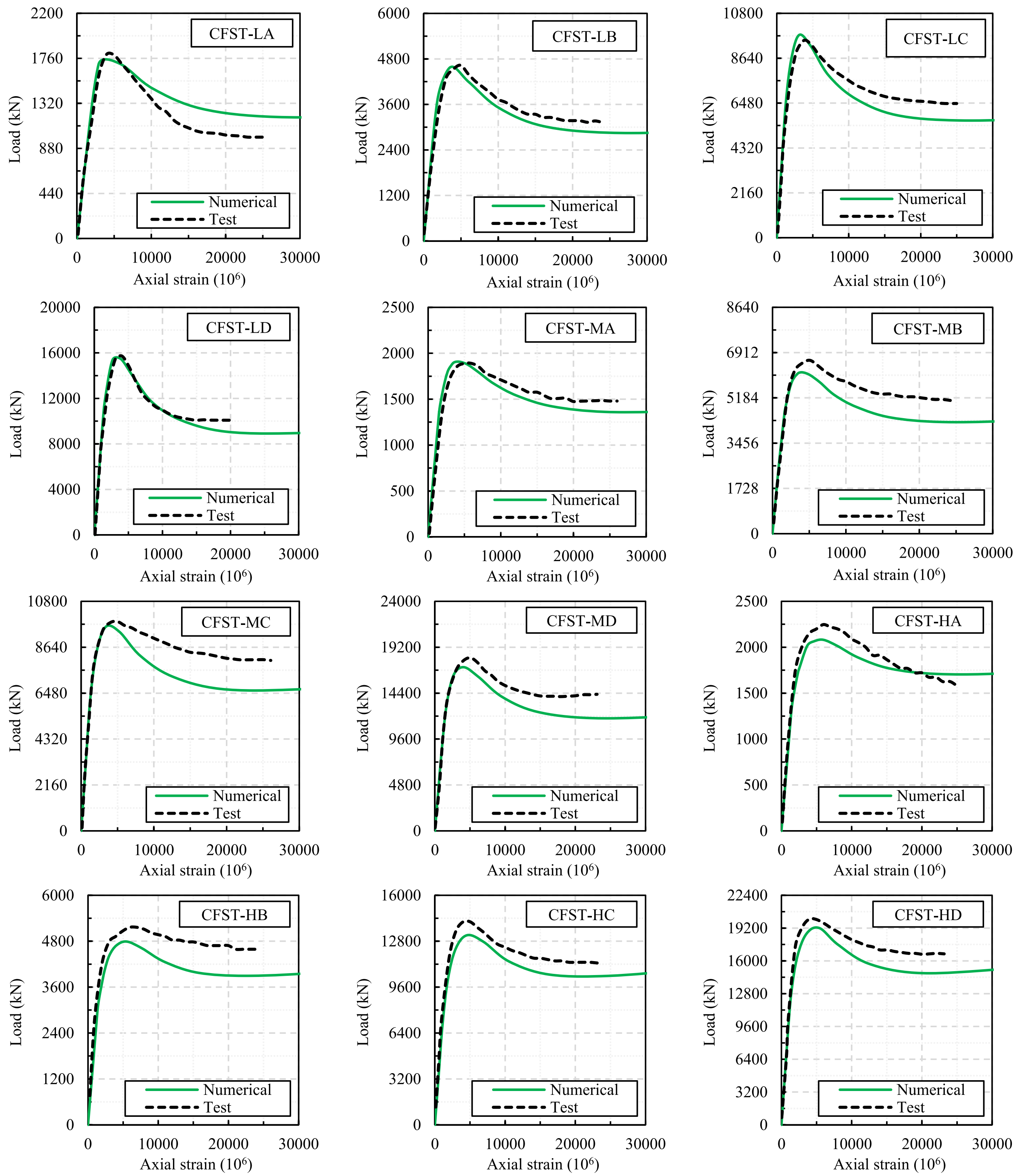


Fig. 5 Load–displacement curves of the numerical models vs. experimental models

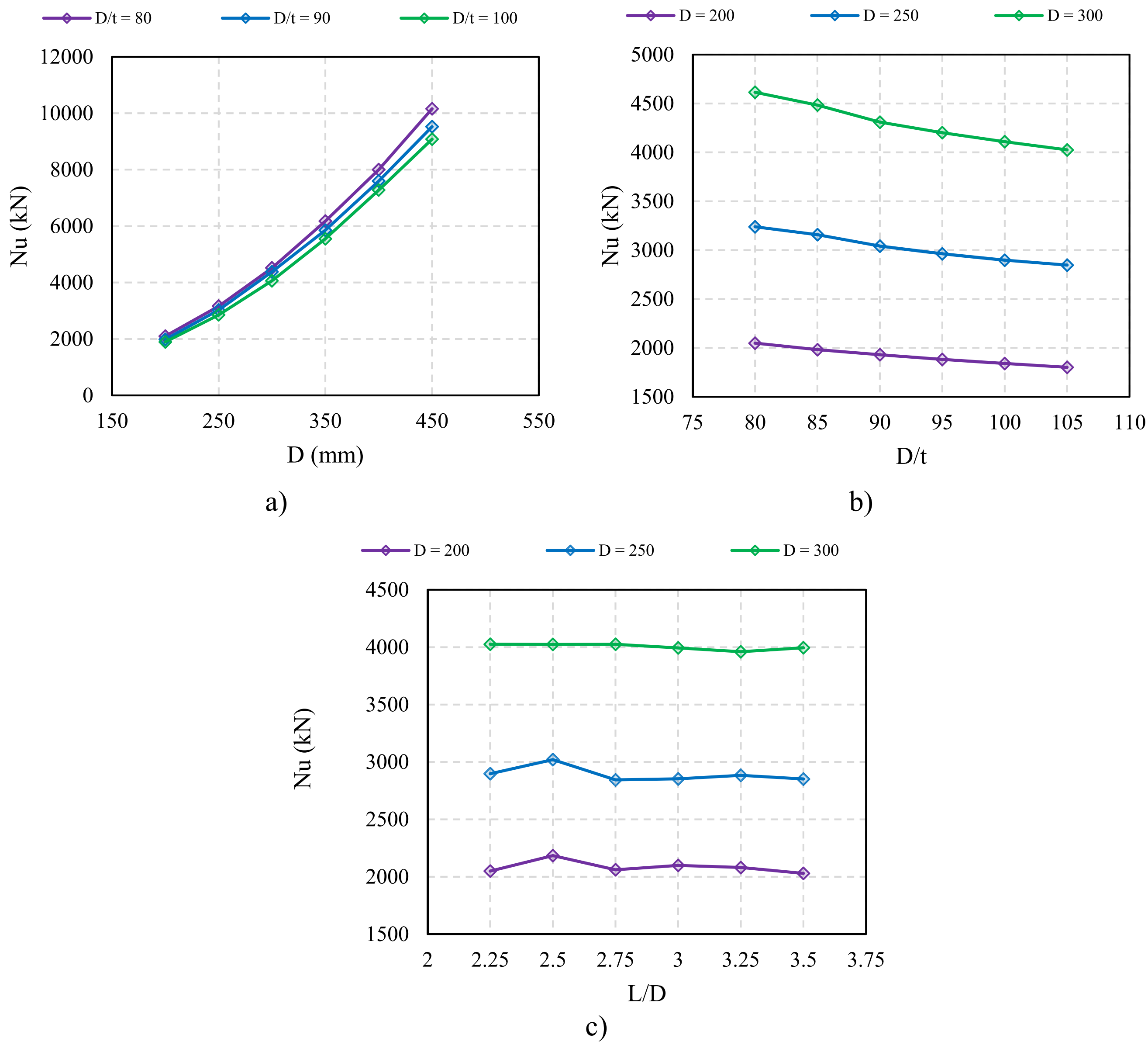


**Fig. 6** Sensitivity analysis of CFST geometric parameters

evaluating the behavior of concrete-filled steel tubes becomes clear, as the models could lead to better resistant estimations than the available design codes.

## 2 Finite Element Modelling

### 2.1 Numerical Model

The study used ABAQUS finite element software to conduct physical-geometric non-linear analyses, considering the plasticity behavior of austenitic stainless steel. The stress–strain relationship properties of the steel used in the study were obtained from [23]. The material behavior was modeled using the two-stage constitutive model from [24] (as shown in Eqs. 1 and 2) based on data retrieved from the literature.

$$\varepsilon = \frac{f}{E} + 0.002\left(\frac{f}{f_y}\right)^n \quad \text{for } f \le f_y \tag{1}$$

$$\varepsilon = \frac{f - f_y}{E_{0.2}} + \left(\varepsilon_u - \varepsilon_{t,0.2} - \frac{f_u - f_y}{E_{0.2}}\right)\left(\frac{f - f_y}{f_u - f_y}\right)^m + \varepsilon_{t,0.2} \quad \text{for } f_y < f \le f_u \tag{2}$$

The Concrete Damaged Plasticity (CDP) constitutive model available in the ABAQUS software was employed to model the behavior of concrete in the study. The confinement behavior of the concrete was considered based on [25],

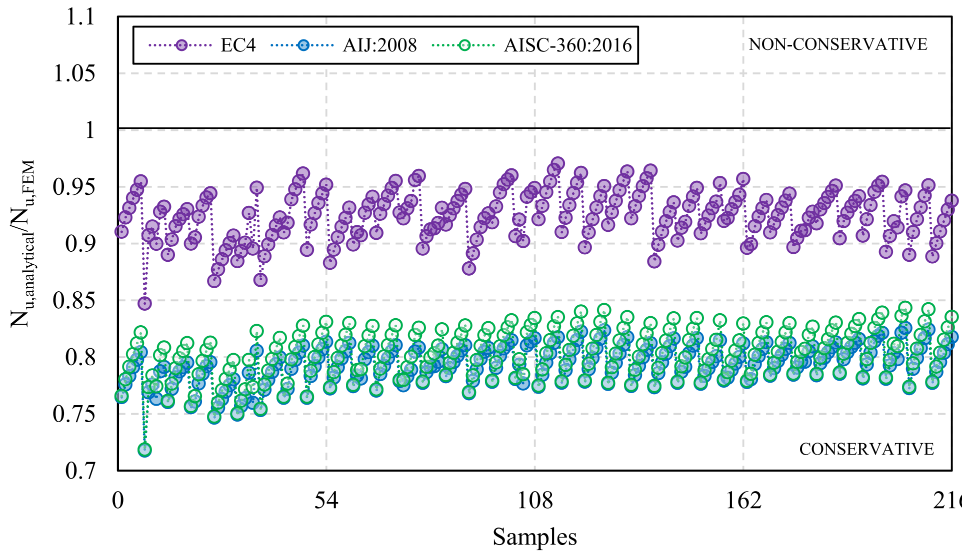


**Fig. 7** Comparison of the numerical results and international design codes

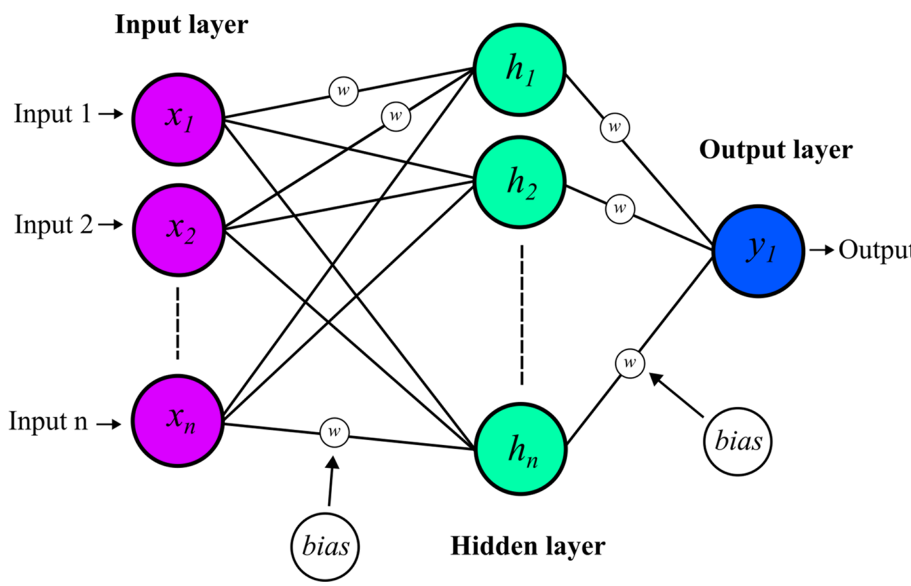


**Fig. 8** Artificial neural network representation

where the authors conducted an extensive survey of experimental data on the compressive behavior of concrete-filled columns and proposed a model using the CDP to account for confinement in CFSTs. The model utilizes typical parameters for circular CFST, such as tube diameter and thickness, concrete strength, and column length, to determine the main properties of CDP (as shown in Eqs. 3–5).

$$\psi = 130\left(\eta + f_c^{\,0.05}\right)^{-6} + 23 \tag{3}$$

$$\frac{f_{b0}}{f_c} = 1.5 f_c^{\,-0.075} \tag{4}$$

$$K_c = \frac{k+2}{2\left(f_c^{\,0.075} + k - 1\right)} \tag{5}$$

The finite element mesh was structured as shown in Fig. 2, with the elements having an average size of D/20, where D is the outer diameter of the column. Solid elements, including C3D6 and C3D8R types, were utilized to model the CFST. For contact properties, it was assumed that the end plates were welded to the outer tube, and therefore, a "tie" constraint was used for these two parts. Surface-to-surface contact was assumed between the concrete and the other constituent parts of the column, such as the external steel tube and end plates. The load was applied to the model by considering a distributed displacement applied to one of the end plates. The Static Riks procedure available in the ABAQUS library was utilized for the analysis. After conducting the analyses, load–displacement curves were generated for each model to obtain the axial resistance capacity of the CFST short columns.

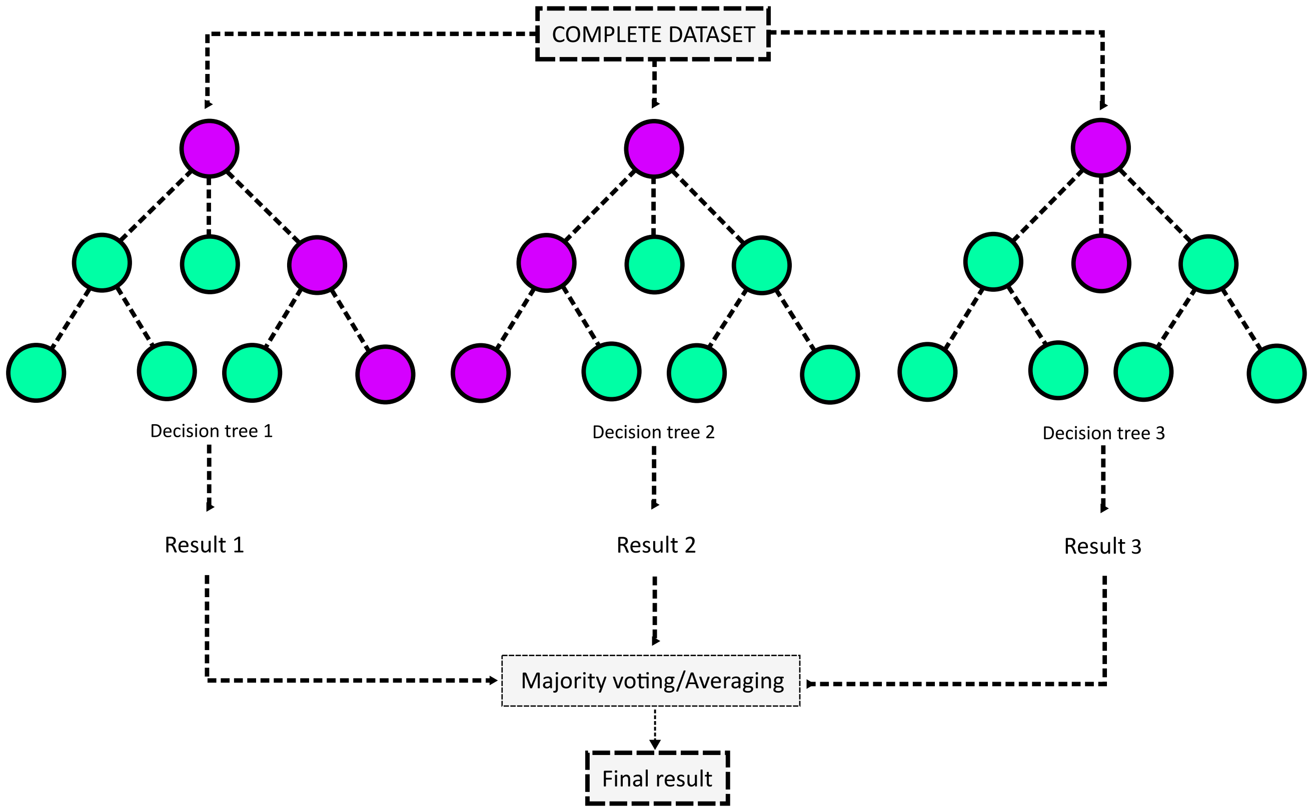


**Fig. 9** Random forest representation

### 2.2 Parametric Study

The study involved creating 216 finite element models of CFST short columns with an outer tube made of austenitic stainless steel. The models were created to evaluate the performance of the structural element under pure axial compression, with different geometric characteristics being considered to cover a wide range of conditions. The diameter of the outer steel tube, the thickness of the steel tubes, the diameter of the concrete section, and the total length of the column were varied. The geometric input data considered in the parametric study is summarized in the flowchart shown in Fig. 3. Notably, the tube thickness and length were normalized based on the diameter of the CFST short-column model. The results obtained from the study allowed for an evaluation of the influence of the geometric properties of the model on the resistant capacity to axial forces of concrete-filled stainless steel tubes, as well as a comparison with design codes to verify their performance in predicting the compression response of CFST columns manufactured with austenitic stainless steel outer tubes.

### 2.3 Validation of the Numerical Model

The validation investigation demonstrated highly satisfactory outcomes. The validation test results are displayed in Fig. 4, while the numerical and experimental load–displacement curves can be found in Fig. 5. The mean error recorded was 1.96% with a standard deviation of 6.65%. In general, the performance of CFST columns was accurately simulated by the finite element analysis.

### 2.4 Sensitivity Analysis and Comparison with Design Codes

The sensitivity analysis revealed that the diameter of the section and the thickness of the steel tube are the most influential parameters on the member's load-carrying capacity (Fig. 6). In contrast, the length of the model had a significantly lesser effect, which was expected due to the nature of the short columns with compact sections studied. In the case of the sections studied, the resistance mechanism is basically due to the achievement of the yielding of the column cross-section, so the main parameters capable of affecting the resistant capacity of the element are the dimensions of its section (diameter and thickness), as well as the maximum stress supported by the materials. It is worth mentioning that

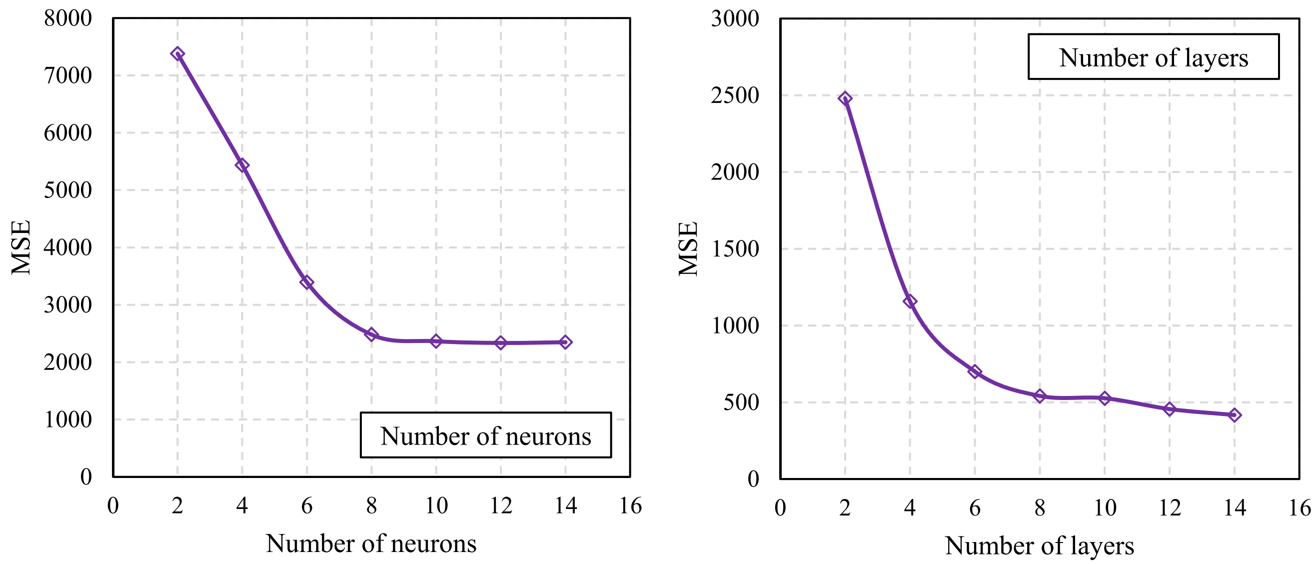


**Fig. 10** Sensitivity study of the number of layers and neurons on the network

**Fig. 11** Activation functions tested

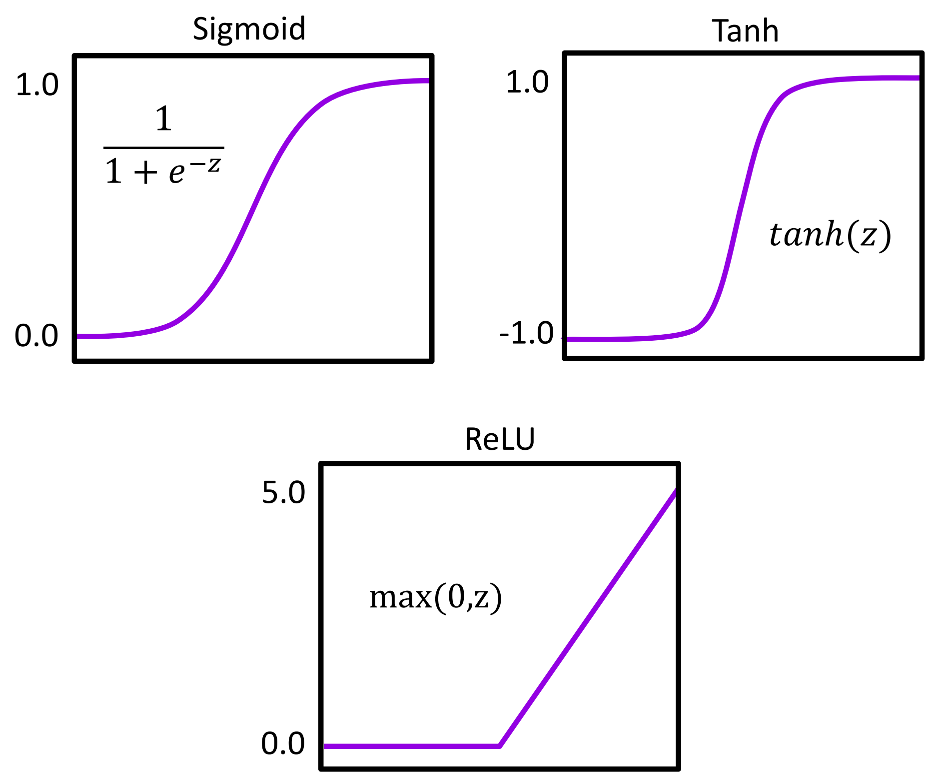


this observation is valid only for the range of length/diameter ratios studied, since the occurrence of failures linked to global instability was not observed in the results, in which the length of the column would play a preponderant role.

Regarding the analysis of design codes, it was observed that the American Standard for Steel Structures (AISC-360) and the Japanese Design Code for concrete-filled steel tubes (AIJ) are overly conservative. In contrast, the European standard for composite structures (EC4) was less conservative but prioritized safety. The superior performance of EC4 can be attributed to its consideration of the confinement effect caused by the concrete inside the tube, which is not considered by the other codes. As a result, EC4 is a more accurate predictor of the behavior of filled composite columns.

Figure 7 illustrates that most of the results obtained from EC4 have a deviation percentage of less than 15% from the numerical results, with an average deviation of 7.55%. Conversely, the other procedures evaluated resulted in deviation

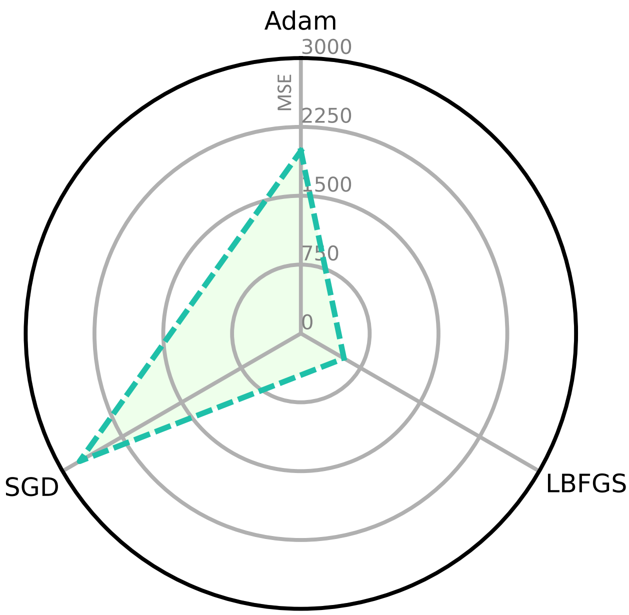


**Fig. 12** Comparison of the training performance according to the optimizer used

percentages greater than 15% and, in some cases exceeding 25%.

## 3 Machine Learning Algorithms

Two different machine learning algorithms were used to model the bearing capacity of short columns of stainless steel tubes filled with concrete: the artificial neural network model and the random forest model.

The neural network model (Fig. 8) consists of layers of interconnected neurons, and each of these neurons is associated with specific weights. Each layer is characterized by a non-linear transformation function, called the activation function, responsible for computing the layer's output based on the provided input, considering the weight associated with the neurons that comprise the respective layer. Input data is organized in the so-called input layer. The layers responsible for the non-linear transformation are called hidden layers. Finally, the output data is organized in the output layer.

The Random Forest model (Fig. 9) is an ensemble-type machine learning algorithm that combines several random decision trees to make predictions. Each decision tree is built using a random sample of the original dataset and a random selection of features to consider for each node split. Final predictions are obtained by voting or averaging the predictions of all individual decision trees. This approach reduces overfitting (a problem that prevents model generalization) and increases the stability and accuracy of predictions compared to a single decision tree.

The information that characterizes the adopted structural member was considered to carry out the training. Thus, the members' geometric characteristics are considered input data, and the axial resistance capacity of the columns was used as output data (training target variable). The data were inserted dimensionally and considered the homogeneity of the adopted units. The input data were separated into training and testing to avoid overfitting in the model. Test data does not participate in training, so machine learning models do not use it to determine the structure of the prediction model. However, these data are used to evaluate the training performance since they are unseen data for the developed model. In this way, it is ensured that the developed model is efficient and can be generalized to new data. The input dataset was split into 70% for training and 30% for testing. This is a usual division in this type of modelling [18, 26, 27].

### 3.1 Artificial Neural Network

It was necessary to perform a sensitivity analysis of the training parameters to apply the neural network model to the dataset developed in the parametric study. The following were evaluated: the number of neurons in the hidden layers, adopting a network with two hidden layers; the number of layers on the model; the type of nonlinear transformation function and the solver responsible for training and determining the weights (this solver is called an optimizer). Figure 10 presents the training performance for the performed sensitivity tests. It is noteworthy that the training performance was evaluated according to the mean squared error (MSE), expressed in Eq. (6). It is also worth mentioning that the input data were normalized according to the mean and standard deviation presented by the dataset used in the training, according to Eq. (7), in which $x_{i,n}$ is the normalized input value, $\mu$ is the mean value of the parameter in the dataset, and $\sigma$ is the standard deviation. This fact considerably facilitates the training process and reduces the time required for completion. The number of neurons was previously determined based on the sensitivity test of the neurons, which was performed with two layers to evaluate the number of layers in the training. It is also noteworthy that given the stochastic nature of the training process, the best MSE values obtained for each situation were used, but considerable variation was observed during the training of the models. As shown in Fig. 10, there is no benefit to the training process in using layers with more than eight neurons. When analyzing the number of layers, it is noted that from eight layers onwards, there is also no considerable improvement in the training results. Thus, a neural network with eight layers of eight neurons each was adopted

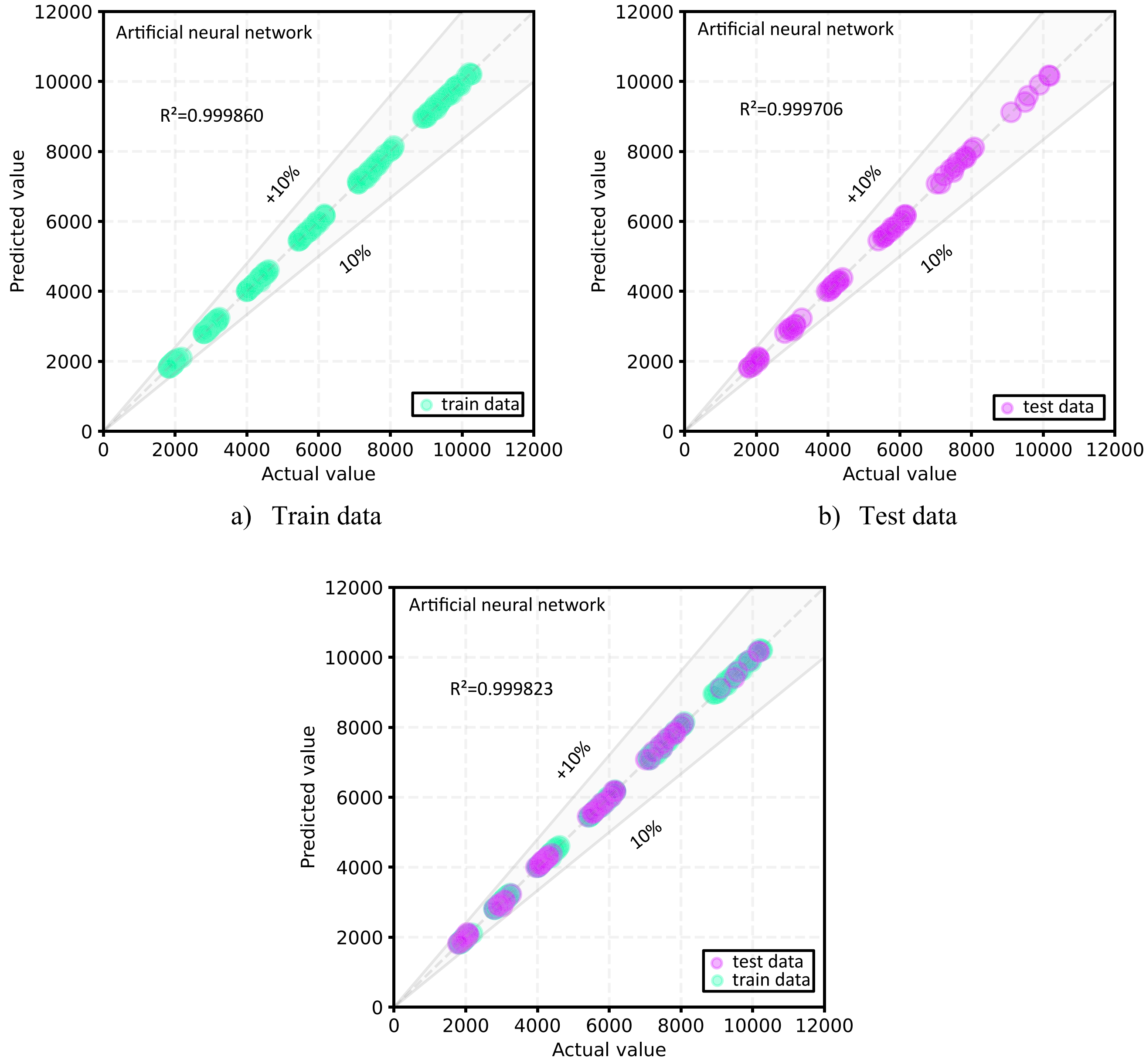


a) Train data

b) Test data

c) Train and test data

**Fig. 13** Results of the artificial neural network modelling

to develop the definitive model.

$$MSE = \frac{1}{n}\left(\sum_{i=1}^{n}(y_i - t_i)^2\right) \tag{6}$$

$$x_{i,n} = \frac{x_i - \mu}{\sigma} \tag{7}$$

Different activation functions were tested for training. However, the one that presented the best results was the ReLU (Rectified linear unit) (Fig. 11a). This function overcomes some limitations of other tested functions, such as Sigmoid and Hyperbolic Tangent (tanh). The sigmoid and tanh functions transform the received input values into values between 0.0 and 1.0 and between -1.0 and 1.0 for the sigmoid function and hyperbolic tangent, respectively. This means that values outside these limits are also transformed to the maximum/minimum value, saturating the responses and leading to inadequate training, depending on the database used as input/output.

Three different optimizers were tested: Adaptive Moment Estimation (Adam), Limited-memory BFGS (LBFGS), and Scaled Gradient Descent (SGD) to evaluate the performance as a function of the type of optimizer used in the analyses. Figure 12 presents the comparison between the results obtained for the training process with the three mentioned models. It is noticed that the optimizer with the best performance in this data set is the LBFGS.

Thus, based on the test performed, a neural network composed of eight layers was adopted, with eight artificial neurons, a ReLU activation function, and an LBFGS optimizer. The results for training are shown in Fig. 13, considering the performance for training data (Fig. 13a), test data (Fig. 13b), and both simultaneously (Fig. 13c). Model performance is evaluated using the $R^2$ metric (Eq. 8), which represents the correlation coefficient between the original data and the data predicted by the model. In Eq. (8) $y_i$ denotes the actual values of the data, $\widehat{y_i}$ denotes the prediction of the machine learning model, and $\overline{y_i}$ is the mean of the input values. An $R^2$ coefficient equal to 1 means a perfect correlation where the predicted data equals the original data. Thus, the closer the $R^2$ of the machine learning model is to unity, the better its performance in predicting the variable studied.

$$R^2 = 1 - \frac{\sum_{i=1}^{n} (\widehat{y_i} - y_i)^2}{\sum_{i=1}^{n} (y_i - \overline{y_i})^2} \tag{8}$$

## 3.2 Random Forest

The calibration study for the training of the random forest model evaluated the number of estimators utilized by the model. By applying various decision trees to the dataset analyzed in this research, it became apparent that exceeding 32 estimators (Fig. 14) does not yield any significant improvement in training.

Therefore, this number was chosen for the final training. The results of the final training are depicted in Fig. 15, indicating good correlation coefficient values for both the training and test data.

As can be seen, when comparing the $R^2$ values for the two training algorithms used, both have excellent correlation, with values close to 1. However, the values observed for training with artificial neural networks were higher. It is worth noting that both models present a more interesting response than that obtained with the design codes. Figure 16 shows a comparison between the correlation coefficients obtained with the standard procedures and with the machine learning models through a Taylor diagram. The diagram makes it possible to verify that the machine-learning models are very close to the reference line, indicating an extremely small deviation from the actual data.

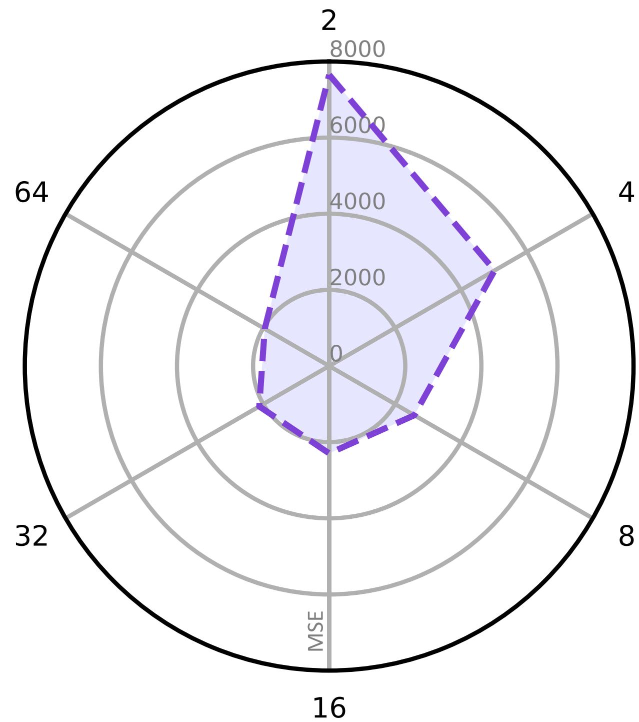


**Fig. 14** Training performance according to the number of estimators

## 3.3 Practical Use of the Models

It was built software responsible for collecting input information from a member, and applying the previously trained machine learning models was created to enable the use of the models. The trained models were saved by serializing the prediction model, which can be read in any programming environment in Python. Therefore, in addition to the column parameters, it is possible to define in the software the model to be used for predicting the bearing capacity of the columns. The software can be downloaded via Github at https://github.com/Adriano-Carvalh0/CFST_AI. Figure 17 presents the software for applying the machine learning models developed in the present study.

# 4 Conclusion

The presented study consisted of a numerical evaluation of the behavior of short CFST columns with compact sections made with austenitic stainless steel outer tubes. The assessment was conducted using the ABAQUS software, in which an extensive parametric study was developed after carrying out a solid validation study. With the validation study, it was possible to verify that the numerical analysis presents an excellent response in simulating the behavior of concrete-filled steel tubes. Through the parametric study results, the influence of the geometric parameters of CFST columns was

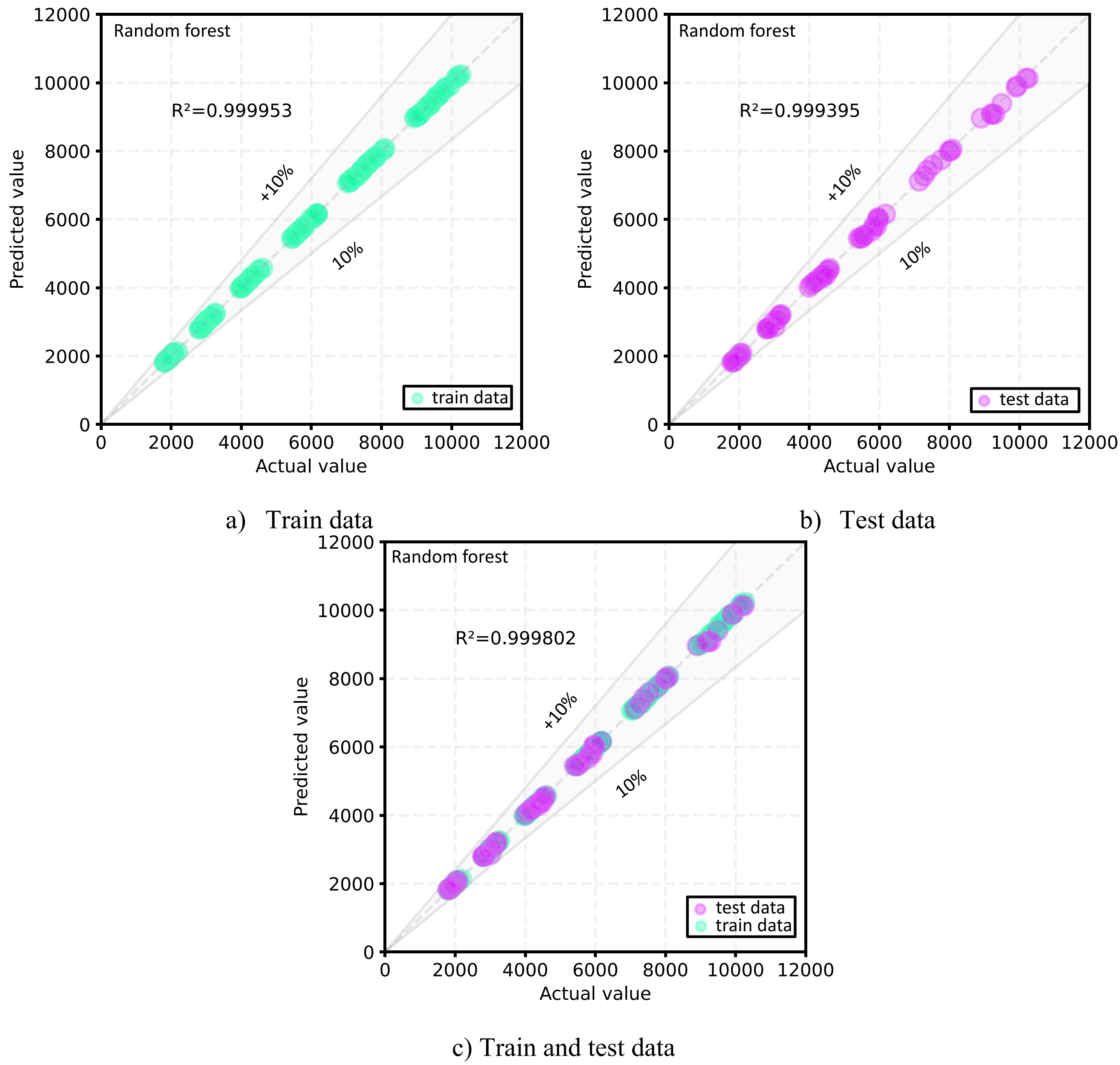


**Fig. 15** Results of the random forest modelling

analyzed, and a comparison with three international design codes was made possible. In addition, based on the database raised about the behavior of the structural element, two different machine learning models were trained, the artificial neural networks and the random forest model.

It was observed that the diameter of the models is the main characteristic that influences the bearing capacity of these members. In addition, it was found that the European standard procedure for composite structures (EC4) has a better capacity (if compared to the other design codes used) to predict the behavior of filled columns since it considers the effect caused by the confinement of the section on this kind of structural member. However, when training the machine learning models, it was found that they had a better response than the design code proposals. It was also verified that the neural networks model presented a better performance in training, although both trained models presented an excellent correlation coefficient with the actual data.

**Fig. 16** Comparison between the machine learning models and the design codes

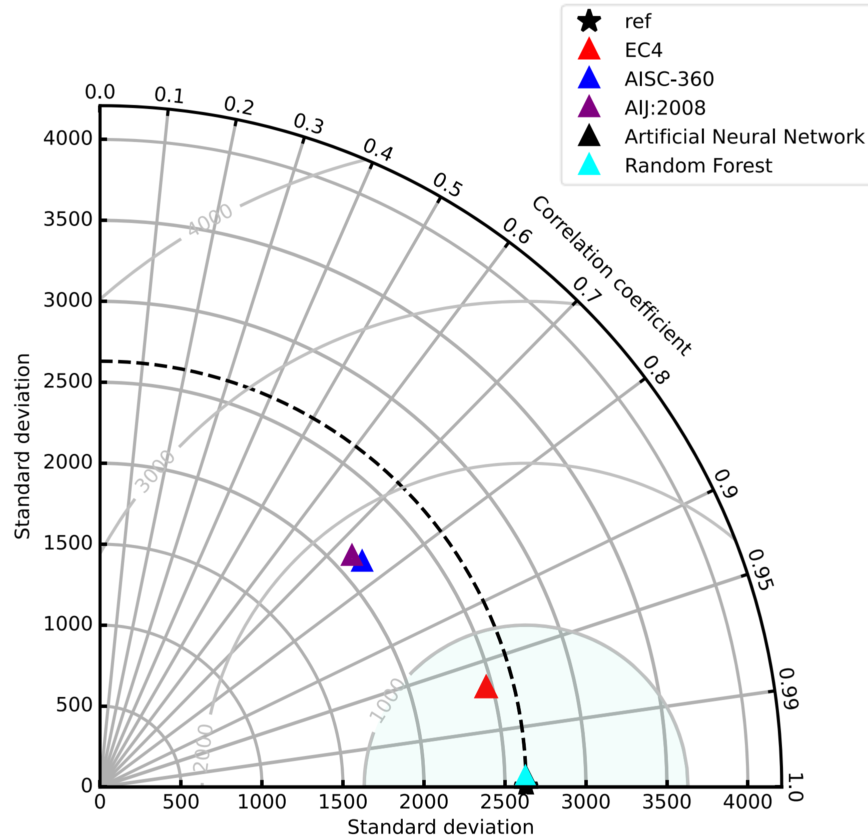


**Fig. 17** Software developed for the application of the trained models

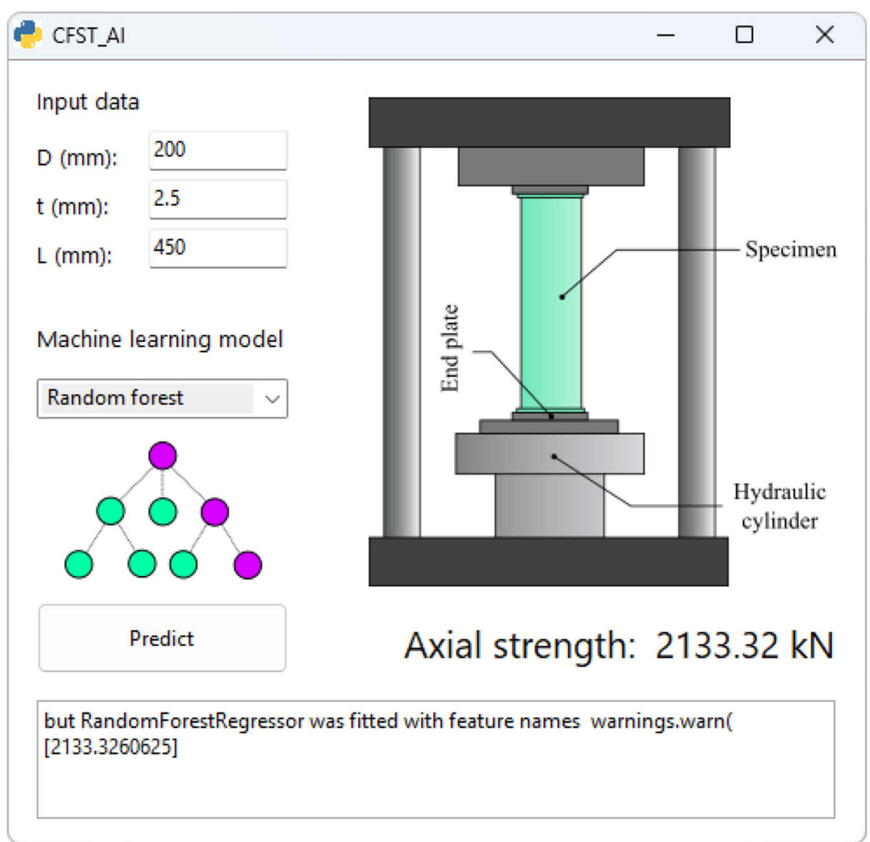

**Acknowledgements** This study was financed by the Coordenação de Aperfeiçoamento de Pessoal de Nível Superior—Brasil (CAPES) – Finance Code 001, and by the Conselho Nacional de Desenvolvimento Científico e Tecnológico (CNPq).

## References

1. İpek, S.; Güneyisi, E.M.: Application of Eurocode 4 design provisions and development of new predictive models for eccentrically loaded CFST elliptical columns. J. Build. Eng. **48**, 103945 (2022). https://doi.org/10.1016/j.jobe.2021.103945
2. Hu, H.; Yang, Z.; Xu, L.; Zhang, Y.; Gao, Y.: Axial compressive behavior of square concrete-filled steel tube columns with high-strength steel fiber-reinforced concrete. Eng. Struct. **285**, 116047 (2023)
3. Mete, E.: Data-driven models for prediction of peak strength of R-CFST circular columns subjected to axial loading. Structures **46**, 1863–1880 (2022)
4. Mete, E.: Data-driven models for prediction of peak strength of R-CFST circular columns subjected to axial loading, vol. 46, pp. 1863–1880 (2022). https://doi.org/10.1016/j.istruc.2022.10.137
5. Dong, H.; Liang, X.; Cao, W.; Zhao, L.; Zhang, J.: Cyclic behavior of circular CFST stub columns with different inner constructions. J. Build. Eng. **53**, 104549 (2022). https://doi.org/10.1016/j.jobe.2022.104549
6. Yang, C.; Gao, P.; Wu, X.; Chen, Y.F.; Li, Q.; Li, Z.: Practical formula for predicting axial strength of circular-CFST columns considering size effect. J. Constr. Steel Res. **168**, 105979 (2020). https://doi.org/10.1016/j.jcsr.2020.105979
7. Zhao, Z.; Mo, S.; Gao, T.: Axial compression capacity of rectangular CFST columns under random pitting corrosion. Structures **48**, 1230–1243 (2023). https://doi.org/10.1016/j.istruc.2023.01.038
8. Liao, J.; Zeng, J.-J.; Long, Y.-L.; Cai, J.; Ouyang, Y.: Behavior of square and rectangular concrete-filled steel tube (CFST) columns with horizontal reinforcing bars under eccentric compression. Eng. Struct. **271**, 114899 (2022). https://doi.org/10.1016/j.engstruct.2022.114899
9. Ekmekyapar, T.; Alwan, O.H.; Hasan, H.G.; Shehab, B.A.; AL-Eliwi, B.J.M.: Comparison of classical, double skin and double section CFST stub columns: Experiments and design formulations. J. Constr. Steel Res. **155**, 192–204 (2019). https://doi.org/10.1016/j.jcsr.2018.12.025
10. Chen, D.; Zha, X.; Xu, P.; Li, W.: Stability of slender concrete-filled steel tubular X-column under axial compression. J. Constr. Steel Res. **185**, 106876 (2021). https://doi.org/10.1016/j.jcsr.2021.106876
11. Chen, D.; Zha, X.; Xu, P.; Zhai, X.: Experimental and theoretical investigation of concrete-filled steel tubular x-column under axial compression. J. Constr. Steel Res. **170**, 106085 (2020). https://doi.org/10.1016/j.jcsr.2020.106085
12. Uenaka, K.: Experimental study on concrete filled elliptical/oval steel tubular stub columns under compression. Thin-Walled Struct. **78**, 131–137 (2014). https://doi.org/10.1016/j.tws.2014.01.023
13. Li, X.; Zhang, S.; Lu, W.; Li, J.: Axial compressive behavior of steel-tube-confined concrete-filled-steel-tubes. Thin-Walled Struct. **181**, 110138 (2022)
14. Teng, J.G.; Huang, Y.L.; Lam, L.; Ye, L.P.: Theoretical model for fiber-reinforced polymer-confined concrete. J. Compos. Constr. **11**, 201–210 (2007). https://doi.org/10.1061/(ASCE)1090-0268(2007)11:2(201)
15. Yang, J.-Q.; Feng, P.: Analysis-oriented model for FRP confined high-strength concrete: 3D interpretation of path dependency. Compos. Struct. **278**, 114695 (2021). https://doi.org/10.1016/j.compstruct.2021.114695
16. Zhang, W.-H.; Wang, R.; Zhao, H.; Lam, D.; Chen, P.: Axial-load response of CFST stub columns with external stainless steel and recycled aggregate concrete: testing, mechanism analysis, and design. Eng. Struct. **256**, 113968 (2022). https://doi.org/10.1016/j.engstruct.2022.113968
17. Wang, Y.; Chen, P.; Liu, C.; Zhang, Y.: Size effect of circular concrete-filled steel tubular short columns subjected to axial compression. Thin-Walled Struct. **120**, 397–407 (2017). https://doi.org/10.1016/j.tws.2017.09.010
18. Rossi, A.; Hosseinpour, M.; Martins, C.H.; Sharifi, Y.: A new formula for predicting lateral distortional buckling strength of I-Beams subjected to different loading conditions. Int. J. Struct. Stab. Dyn. **22**, 1–29 (2022). https://doi.org/10.1142/S0219455422501292
19. Amayreh, L.; Saka, M.P.: Failure load prediction of castellated beams using artificial neural networks. Asian J. Civ. Eng. (Build. Hous.) **6**, 35–54 (2005)
20. Liu, D.; Bao, Y.; Li, H.: Machine learning-based stochastic subspace identification method for structural modal parameters. Eng. Struct. **274**, 115178 (2023). https://doi.org/10.1016/j.engstruct.2022.115178
21. Schweigler, M.; Bader, T.K.; Hochreiner, G.; Unger, G.; Eberhardsteiner, J.: Load-to-grain angle dependence of the embedment behavior of dowel-type fasteners in laminated veneer lumber. Constr. Build. Mater. **126**, 1020–1033 (2016). https://doi.org/10.1016/j.conbuildmat.2016.09.051
22. Shafighfard, T.; Bagherzadeh, F.; Rizi, R.A.; Yoo, D.-Y.: Data-driven compressive strength prediction of steel fiber reinforced concrete (SFRC) subjected to elevated temperatures using stacked machine learning algorithms. J. Mater. Res. Technol. **21**, 3777–3794 (2022). https://doi.org/10.1016/j.jmrt.2022.10.153
23. Afshan, S.; Zhao, O.; Gardner, L.: Standardised material properties for numerical parametric studies of stainless steel structures and buckling curves for tubular columns. J. Constr. Steel Res. **152**, 2–11 (2019). https://doi.org/10.1016/j.jcsr.2018.02.019
24. Rasmussen, K.J.R.: Full-range stress-strain curves for stainless steel alloys. J. Constr. Steel Res. **59**, 47–61 (2003)
25. Lin, S.; Zhao, Y.: Numerical study of the behaviors of axially loaded large-diameter CFT stub columns. J. Constr. Steel Res. **160**, 54–66 (2019). https://doi.org/10.1016/j.jcsr.2019.05.020
26. Hosseinpour, M.; Rossi, A.; Sander, A.; De Souza, C.; Sharifi, Y.: New predictive equations for LDB strength assessment of steel – concrete composite beams. Eng. Struct. **258**, 114121 (2022). https://doi.org/10.1016/j.engstruct.2022.114121
27. de Carvalho, A.S.; Hosseinpour, M.; Rossi, A.; Martins, C.H.; Sharifi, Y.: New formulas for predicting the lateral–torsional buckling strength of steel I-beams with sinusoidal web openings. Thin-Walled Struct. **181**, 110067 (2022). https://doi.org/10.1016/j.tws.2022.110067